

Structural characteristics and physicochemical properties of starches from winter squash (*Cucurbita maxima* Duch.) and pumpkin (*Cucurbita moschata* Duch. ex Poir.)

Tiantian Yuan, Fayin Ye^{*}, Ting Chen, Mengsa Li, Guohua Zhao

College of Food Science, Southwest University, Chongqing, 400715, People's Republic of China

ARTICLE INFO

Keywords:

Pumpkin
Starch
Structural properties
Functional properties
Digestibility

ABSTRACT

Winter squash (*Cucurbita maxima* Duch.) and pumpkin (*Cucurbita moschata* Duch. ex Poir.) are widely consumed in the world. Empirical evidences showed that their cooked texture was related to the starch content and probably starch properties. In this study, starches were extracted from 2 winter squash cultivars (Yinli and Heili) and 1 pumpkin cultivar (Miben) popularly cultivated in China. The mature fruits of three cultivars contained 1.05–6.47% (fresh weight) starch with different granule sizes (d (0.5) 9.51–15.18 μm). Starches from winter squash and pumpkin had polyhedral and spherical shape granules with amylose content varied from 21.35% to 30.17%. All starches exhibited B-type crystalline structure. The relative crystallinity ranged from 26.15% to 31.31%, and the IR absorbance ratios of 1022/995 cm^{-1} and 1045/1022 cm^{-1} ranged from 0.759 to 0.806 and from 0.565 to 0.607, respectively, among 3 cultivars. SAXS pattern indicated 9.59–9.80 nm D_{Bragg} for these starches. The M_w was highest (5.03×10^7 g/mol) in Miben starch but lowest (3.64×10^7 g/mol) in Heili starch. All starches had identical amylopectin branch chain distributions but varied in average chain length and f_{b1} and f_{b2} chains. The gelatinization temperature (T_g , T_p , T_c) and enthalpy change (ΔH) were lowest in Heili starch and highest in Miben starch. The peak, trough, final and setback viscosities varied from 4468 to 6266 cP, 3116 to 4259.5 cP, 4075 to 6073 cP, and 787 to 1813 cP, respectively. All starch granules showed strong resistance to enzymatic hydrolysis. Yinli and Miben starches had higher RS content in starch pastes and retrograded gels than Heili starch.

1. Introduction

Winter squash (*Cucurbita maxima* Duch.) and pumpkin (*Cucurbita moschata* Duch. ex Poir.) are two of the most commercially cultivated *Cucurbita* species throughout the world (Zou et al., 2019). Owing to the nutritive value and bioactive benefits, the flowers, fruit, leaves, and seeds of squashes and pumpkins are eaten as a vegetable or traditionally used for medicinal purposes (Rolnik & Olas, 2020). Among them, the fruit of squash and pumpkin is usually consumed by simply boiling, steaming or baking, or processed to formulate pies, jams, juice and soups in some countries (Rolnik & Olas, 2020). To extend its use, the flesh of fruit is dried and ground into flours, which is explored as an ingredient for bread, cakes and other bakery products (Al-Ghamdi, Hong, Qu, & Sablani, 2020; Nakhon, Jangchud, Jangchud, & Prinyawiwatkul, 2017). Practically, pumpkin peels are a low cost source for extracting pectin (Jun, Lee, Song, & Kim, 2006). Pumpkin seeds from some cultivars are

baked or roasted for culinary purposes or used as good source for oil and protein extraction (Rezig et al., 2013).

Starch is a major component of some vegetable foods such as potato, pumpkin, yam, sweet potato, taro, lotus root and water chestnut. Its structural and physicochemical properties have a marked impact on the quality of cooked or processed vegetable foods. The understanding of starch properties can help us to unravel the mechanism of food quality formation during the processing process, which is the premise of developing starchy vegetable products or ingredients. Firstly, starch as a component has an important influence on the texture, flavor and taste of starchy vegetables. Starch in tissues undergoes gelatinization during cooking or thermal treatment, which results in microstructural and textural change of starchy vegetable foods. Corrigan, Hurst, and Potter (2001) reported that the texture of squash fruit was related to its starch content and its properties. Secondly, the technical properties of starch are a key factor guiding the choosing of raw materials for formulating

^{*} Corresponding author. College of Food Science, Southwest University, No.2 Tiansheng Road, Beibei, Chongqing, 400715, People's Republic of China.
E-mail address: fye@swu.edu.cn (F. Ye).

starchy vegetable products (Hu, Li, Regenstein, & Wang, 2019). Reyniers, Vluymans, et al. (2020) recently showed that the structure of amylose determined the strength of potato flake based dough sheet and its expansion properties when subjected to deep-frying. Results indicated that the level of amylose of intermediated chain length was highly responsible for the texture of potato flake based crisp. In addition, the suitability of potato flakes for crisp making could be improved by controlled amylolysis (Reyniers, De Brier, et al., 2020). Thirdly, starch and its change in processing or storage affect the nutritional and glycaemic properties of starchy vegetable foods (Zhao, Andersson, & Andersson, 2018). Chen, Singh, and Archer (2018) found that retrogradation of potato starch in cooked tuber increased the relative crystallinity and lowered the starch digestibility of the stored tuber samples.

Starch is the major component in pumpkin flesh and may amount up to 60% of the dry weight (Hurst, Corrigan, Hannan, & Lill, 1995). It is expected that the property of starch is the determinative factor in the quality of pumpkin flesh or pulp based food products. Stevenson, Yoo, Hurst, and Jane (2005) isolated and characterized the starches from winter squash (*Cucurbita maxima* D.) fruit at harvest. The starches from winter squash exhibited a B-type X-ray diffraction pattern and relative crystallinity in range of 35%–55.7%. The amylose content of starches from pumpkin varied from 28.94% to 32.79% depending on cultivars (Przetaczek-Rożnowska, 2017). The potential of pumpkin starch in food industry and human wellness has been limited recognized with studies performed on the properties such as physicochemical, functional and nutritional importance. As reported by Przetaczek-Rożnowska (2017), pumpkin starch pastes exhibited over four times higher final viscosity than corn starch pastes and pumpkin starch gels displayed markedly better texture properties than potato or corn starch gels. In order to improve the functionality of pumpkin starch, Rożnowski, Przetaczek-Rożnowska, and Boba (2016) studied the phosphorylation of pumpkin starch, and concluded that the phosphorylated pumpkin starch displayed lower pasting temperature and less susceptibility to retrogradation when compared to unmodified ones. Bai, Zhang, Chandra Atluri, Chen, and Gilbert (2020) recently evaluated the *in vitro* digestibility of pumpkin flours and concluded that it could be affected by the molecular structure, content and distribution of both starch and pectin components. However, as an unusual starch source, the pumpkin starch is still underexploited. The above-mentioned reports urge a deep understanding of the diverse aspects of pumpkin starch for more efficient utilization. The present work mainly aims to tap the molecular, structural and functional properties of starches from two cultivars of winter squash (*Cucurbita maxima* Duch.) and one cultivars of pumpkin (*Cucurbita moschata* Duch. ex Poir.) commonly found in South China. The *in vitro* digestibility of RDS, SDS, and RS was compared between raw, gelatinized and retrograded pumpkin starches of different cultivars. This study will help the food industry to explore its use for technological and nutritional applications. Moreover, further investigations will benefit from our results such as enhancing the functional properties of the studied starches by some modification processing.

2. Materials and methods

2.1. Materials

The mature fruits of two winter squash (*Cucurbita maxima* Duch.) varieties i.e., Yinli (about 1–2 kg) and Heili (about 1–1.5 kg), and one pumpkin (*Cucurbita moschata* Duch. ex Poir.) cultivar Miben (about 1.5–2.5 kg), were purchased from a local supermarket in Chongqing, China. Amyloglucosidase (3300 U/mL) and glucose oxidase/peroxidase (GOPOD) assay kit were purchased from Megazyme (Wicklow, Republic of Ireland). The porcine pancreatic α -amylase (≥ 5 U/mg solid) and heat stable α -amylase (3000 U/mL) were purchased from Sigma-Aldrich Co. (Shanghai, China). Other reagents used in the experiment were of analytical grade.

2.2. Starch extraction

Starch was extracted using the method described by Przetaczek-Rożnowska (2017) with some modifications. The pumpkin fruits were washed and cut into small pieces. A beater (JYL-C16D, Joyoung, China) was used to smash the pieces into pulp. The pulp was then filtered with a piece of gauze (100-mesh). The filtrate was centrifuged at $3760 \times g$ for 20 min. The supernatant was discarded and the colored substances on the top of the sediment were scraped off. The sediment was washed three times with deionized water and dried in an oven at 40°C for 24 h. Dried starches were stored in plastic bags and sealed for further analysis.

2.3. Color analysis

The determination of instrumental color parameters was performed by using a colorimeter (UltraScan PRO, HunterLab, Reston, USA). The color parameters of starches was expressed as L^* , a^* and b^* , reflecting lightness, redness/greenness and yellowness/blueness, respectively.

2.4. Chemical analysis and measurement of apparent amylose content

The content of total starch was measured with glucose oxidase–peroxidase reagent (GOPOD) assay kit following AOAC method 996.11 (2000). The moisture content was analyzed by gravimetric (method 945.46; AOAC, 2006). Protein, lipid and ash contents were determined by AOAC standard methods 955.04 (2000), 960.39 (2000) and 923.03 (2000), respectively.

Apparent amylose content of winter squash and pumpkin starches was measured following the method of Zobot, Silva, Emerick, Felisberto, and Meireles (2018) with some modifications. Briefly, the sample was firstly subjected to methanol extraction for fat removal, then 100 mg starch sample (dry basis), 1 mL absolute ethanol and 9.0 mL 1 mol/L NaOH were introduced into a 150 mL Erlenmeyer flask. The flask was heated in boiled water for 10 min, after that the sample was cooled and transferred into a volumetric flask (100 mL). Deionized water was added to the flask until the liquid volume up to 100 mL. Five milliliters of sample solution was transferred into a volumetric flask within about 50 mL deionized water. Then 1 mL acetic acid (1 mol/L) was added into this volumetric flask and mixed thoroughly by shaking intensely. By adding 2 mL iodine (0.2% I_2 and 2% KI, w/v) to the volumetric flask, the liquid volume was adjusted to 100 mL. The volumetric flask was shaken for a few seconds and stood still for 10 min. The absorbance value at 720 nm was recorded by a UV-spectrophotometer (UV-5100, Metash, China). The apparent amylose content was calculated by the calibration curve.

2.5. Optical microscope observation and field scanning electron microscopy

The optical image of starch samples were taken under an Olympus BX53 microscope with polarized light accessory. The starch was dispersed in 50% glycerol (1%, w/v), and the dispersion was dropped on the slide and covered with the cover slip. The slide was placed on the stage for observation. The observation mode was transformed between bright field and polarized light.

The morphology of winter squash and pumpkin starch granules were observed by using a field emission scanning electron microscopy (JSM-7800F, JEOL, Japan) at an accelerating voltage of 1–3 kV. Before examination, the samples were dispersed in ethanol and volatilized completely on the foil at room temperature. The foil with starch particles was stick to the stage with double-sided tape and then coated with gold. The images were captured at the magnification of $3000 \times$.

2.6. Particle size distribution measurement

A laser diffraction particle size analyzer (Mastersizer 2000; Malvern, UK) was used to measure the particle size of starch samples. The starch sample was dispersed in deionized water. The dispersion was added into a beaker under the condition of 2000 r/min until the opacity between 10% and 11% (Guo et al., 2019). The refractive index of water and starch were set to 1.33 and 1.52 (Li et al., 2020). Median diameter $d(0.5)$ and the volume-weighted mean diameter $D[4,3]$ were recorded (Lin et al., 2016).

2.7. Molecular weight distribution and chain length distributions

The molecular weight distribution of winter squash and pumpkin starches were analyzed by means of gel permeation chromatography-refractive index-multi-angle laser light scattering detection (GPC-RIMALLS) techniques. The starch sample (5 mg) was dissolved in 1 mL dimethyl sulfoxide (DMSO) in a 60 °C bath with vigorously shaking. The mixture was centrifuged (14 000 r/min, 10 min) and the supernatant (100 μ L) of that was injected into the system. Details of experimental condition were as the following: the refractive index detector: Optilab Trex (Wyatt technology, CA, USA), the multi-angle laser light scattering detector: DAWN HELEOS II (Wyatt technology, CA, USA); analytical columns: Ohpak SB-805 HQ (300 \times 8 mm), Ohpak SB-804HQ (300 \times 8 mm), Ohpak SB-803 HQ (300 \times 8 mm); column temperature: 65 °C; mobile phase: 5 mM LiBr, DMSO; flow rate: 0.4 mL/min. The data was analyzed by the Astra version 6.1 software.

The chain length distribution of amylopectin was determined by the high-performance anion-exchange chromatography system (HPAEC-PAD, ICS500+, Thermo Fisher Scientific, USA) coupled with a pulsed amperometric detector (PAD). 5 mg starch sample was dissolved into deionized water and incubated 60 min at boiling water with intermittent vortex mixing. The gelatinized starch (2.5 mL) was mixed with CH_3COONa (125 μ L), NaN_3 (5 μ L) and isoamylose (5 μ L) and incubated at 38 °C for 24 h. Then, 600 μ L of mixture solution was sampled and subsequently dried with a flow of nitrogen. The sample was dissolved in the mobile phase (600 μ L) and centrifuged (12 000 r/min, 5 min). The supernatant (20 μ L) was injected into the system. Details of experimental condition were as follows: analytical column: Dionex™ CarboPac™ PA10 (250 \times 4.0 mm, 10 μ m); mobile phase A: 200 mM NaOH; mobile phase B: 200 mM NaOH/200 mM NaAC; column temperature: 30 °C. The flow rate was set as 0.3 mL/min. The peak areas corresponding to different branch chain lengths were examined using a PeakNet software (Dionex, Sunnyvale, USA) and the results were expressed as the relative area versus degree of polymerization (DP).

2.8. Attenuated total reflectance-Fourier transforms infrared spectroscopy (ATR-FTIR)

ATR-FTIR spectra of Yinli, Heili and Miben starches were recorded on a PerkinElmer Spectrum 100 with a universal ATR sampling accessory. The numbers of scans were set to 32 with a resolution of 4 cm^{-1} from 600 cm^{-1} to 4000 cm^{-1} .

2.9. X-ray diffraction (XRD)

The crystalline structures of Yinli, Heili and Miben starches were analyzed by using the X'Pert3 Powder XRD system (PANalytical, Almelo, the Netherlands). Prior to analysis, the starch samples were equilibrated at 40 °C for 24 h and the moisture of all samples were 9.02% \pm 0.25%. The power of Cu-K α radiations for X-ray diffractometer was 1600 W (40 kV \times 40 mA). The starch sample was scanned at diffraction angle (2θ) from 4° to 40° at the scanning speed of 2°/min. The relative crystallinity was the ratio of the crystallinity area to the total diffraction area with MDI-Jade 5.0 software (Material Data, Inc., Livermore, CA, USA).

2.10. Small angle X-ray scattering (SAXS)

The SAXS experiment was carried out at 1W2A SAXS station at the Beijing Synchrotron Radiation Facility (BSRF). The electron energy was 2.5 GeV and the beam current is about 180 mA. The distance between the sample and the detector is 1564 mm, and the wavelength of synchrotron radiation is 0.154 nm. Hydrated starches with concentrations of ca. 40% were prepared according to the method of Qiao et al. (2019). The 1D scatter photo obtained by the SAXS device was converted into a 2D image and parameters was analyzed by using Fit2d software. The scattering vector, q (nm^{-1}), was defined as $q = 4\pi\sin\theta/\lambda$ (2θ , scattering angle).

2.11. Differential scanning calorimetry (DSC)

The thermal properties of Yinli, Heili and Miben starches were examined by DSC (PerkinElmer & Co, USA). Starch and deionized water at a ratio of 1:2 were weighted into an aluminum pan (Φ 5.4 \times 2.0 mm) and sealed. The sample was equilibrated overnight at room temperature so that starch was thoroughly hydrated. The slurry was heated from 20 °C to 120 °C at 10 °C/min. The onset (T_o), peak (T_p), and conclusion (T_c) temperatures as well as enthalpy of gelatinization (ΔH) were analyzed by TA Instruments TRIOS version 4.4. 0.

2.12. Rapid viscosity analyzer

Rapid viscosity analyzer (RVA-TecMaster, Perten Instruments, Sweden) was used to measure the pasting properties of Yinli, Heili and Miben starches. Starch slurry (10%, db; 28 g of total weight) was prepared and placed in a sample test canister. Samples were equilibrated 1 min at 50 °C, heated to 95 °C at a rate of 10 °C/min, held at 95 °C for 2.5 min and cooled down to 50 °C at a rate of 12 °C/min. The pasting parameters including peak temperature (PT), time to peak viscosity (TTPV), peak viscosity (PV), trough viscosity (TV), final viscosity (FV), and breakdown (BD) and setback (SB) viscosities were output through TCW 3 software.

2.13. Enzymatic hydrolysis analysis of starch

A centrifuge tube weighted with 100 mg of starch granules and 5 mL of sodium acetate buffer (0.2 mol/L, pH 5.2) was placed overnight at room temperature, followed by incubating at 37 °C in water bath for 10 min. Then 10 mL of freshly prepared enzyme solution containing porcine pancreatic α -amylase (290 U/mL) and amyloglucosidase (15 U/mL) was added into the centrifuge tube. The centrifuge was incubated in a constant temperature oscillation water bath cabinet (DKZ-3B, Shanghai, China) at 37 °C up to 1200 min. 0.5 mL of the digested solution was sampled at each time point (0, 20, 120, 600, 1200 min) and mixed with 2 mL absolute ethanol to terminate the digestion. The amount of released glucose in the digestion solution was quantified by using a glucose oxidase/peroxidase (GOPOD) assay kit (Megazyme, Wicklow, Republic of Ireland). The percentage of digested starch was calculated according to the method of Qiao et al. (2019). Furthermore, the enzymatically degraded starch granules were subjected to morphology and lamellae structure characterization according to the methods described in Section 2.5 and 2.10.

2.14. In vitro digestion analysis of starch

For the determination of rapidly digestible starch (RDS), slowly digestible starch (SDS) and resistant starch (RS), *in vitro* digestion of native, gelatinized and retrograded starches was performed following the method Guo et al. (2019) with some modifications. Briefly, 100 mg starch sample was suspended in 5 mL H_2O and heated in boiling water for 1 h to prepare the gelatinized starch. Then, the gelatinized starch was stored for 48 h at 4 °C to prepared retrograded starch. The starch sample

(2%, w/v) was incubated in 10 mL enzyme solution (0.2 M, pH 5.2 sodium acetate buffer; 2900 U of porcine pancreatic α -amylase; 150 U of amyloglucosidase) in a constant temperature oscillation water bath cabinet (DKZ-3B, Shanghai, China) at 37 °C with constant shaking. The digestion was terminated by adding 4 vol of absolute ethanol and centrifuged at 4000 r/min for 10 min. The amount of glucose in the supernatant was quantified using GOPOD assay kit (Megazyme, Wicklow, Republic of Ireland). RDS (digested within 20 min), SDS (digested between 20 and 120 min) and RS (undigested after 120 min) were calculated according to the method of Englyst, Kingman, and Cummings (1992).

2.15. Statistical analysis

The determinations were performed in triplicate and results were expressed as mean \pm standard deviation (SD). One-way analysis of variance (ANOVA) followed by Duncan's multiple-range tests were carried out using the SPASS 26.0 statistical software. Mean values were considered significantly different at $p < 0.05$.

3. Results and discussion

3.1. General aspects of starches isolated from winter squash and pumpkin fruits

In this study, the content of starch for three cultivars, Yinli, Heili and Miben, was 6.47g/100 g (fresh weight; FW), 1.05 g/100 g (FW) and 3.13 g/100 g (FW), respectively. Previous study indicated that pumpkin fruits contained different levels of starch, varying from 0.49 to 9.22 g/100g (FW) for low-starch content cultivars to 7.76–16.27 g/100g (FW) for high-starch content cultivars (Corrigan et al., 2001). Except for cultivars, the content of starch varies for many factors. Corrigan et al. (2001) reported that the starch content for winter squash was markedly decreased during the storage periods. It is worthy to note that the starch content affected the texture properties of cooked pumpkin fruits (Corrigan et al., 2001). The pumpkin fruit presented different sweet and mealy (dry) taste according to the level of dry matter and starch content (Hurst et al., 1995).

The starch samples extracted from Heili, Yinli and Miben are powders in pale color. The color analysis of these samples was done by an Ultrascan colorimeter (Hunterlab, USA) and the data was presented in Table 1. Miben starch showed significantly ($p < 0.05$) higher L^* than Heili and Yinli starches, indicating Miben starch was whiter or lighter than the other two starches. Moreover, Heili starch showed lowest a^* value and highest b^* value, implying it was more towards greenness and yellowness. The impurities such as pigments adsorbed onto the granules of starch were responsible for the greenness and yellowness of the starch samples (Nakhon et al., 2017).

The winter squash and pumpkin starches exhibited a mixture of polyhedral and spherical granules with varying in size (Fig. 1). Under polarized light microscopy, these starches showed typical birefringence (Maltese cross) with the hila in the center of granules. The birefringence was due to the differences in refractive index and density of amorphous and crystalline regions in starch granules (Liu, Jiang, Liu, Li, & Li, 2021). Previous studies showed that the intensity of birefringence was related to the granule size, crystallinity index, and microcrystalline orientation of starch (Zhang, Li, Liu, Xie, & Chen, 2013). For the each starch sample studied, the birefringence patterns of larger granules were much stronger and clearer than the smaller ones. This phenomenon was probably due to higher order of crystallite organization in larger granules of pumpkin starch (Liu et al., 2021).

The morphology of the winter squash and pumpkin starch granules was observed by scanning electron micrographs (Fig. 1). It can be seen that Miben starch consisted of spherical granules as well as some dome-shaped granules, which were similar to the starch isolated from the pumpkin (*Cucurbita moschata* L.) (Nakhon et al., 2017). However, Yinli

Table 1

General characteristic of starches extracted from the winter squash and pumpkin fruits ^a.

Parameters	Cultivars		
	Yinli	Heili	Miben
Color values ^b			
L^*	96.50 \pm 0.15b	95.61 \pm 0.42c	97.58 \pm 0.35a
a^*	1.62 \pm 0.04a	1.32 \pm 0.08b	1.60 \pm 0.03a
b^*	2.47 \pm 0.13b	3.56 \pm 0.05a	2.32 \pm 0.06b
Granule size distribution ^c			
d (0.5) (μ m)	15.18 \pm 0.22a	9.51 \pm 0.32c	12.46 \pm 0.02b
D [4,3] (μ m)	45.14 \pm 1.11a	33.10 \pm 1.61b	21.95 \pm 0.15c
Specific surface area (m^2/g)	0.60 \pm 0.01b	0.98 \pm 0.12a	0.85 \pm 0.00a
Proximate composition ^d			
Total starch (% db)	91.56 \pm 0.62a	87.87 \pm 1.59a	92.73 \pm 3.42a
Apparent amylose (% db)	30.17 \pm 0.48a	26.36 \pm 0.29b	21.35 \pm 0.06c
Moisture (% wb)	15.90 \pm 0.17a	14.69 \pm 0.02b	13.36 \pm 0.61c
Lipid (% db)	1.01 \pm 0.08a	1.38 \pm 0.14a	1.21 \pm 0.12a
Protein (% db)	0.16 \pm 0.03c	0.47 \pm 0.05b	0.89 \pm 0.04a
Ash (% db)	0.19 \pm 0.00a	0.29 \pm 0.06a	0.25 \pm 0.04a
Molecular weight ^e			
M_n (kg/mol)	19308.90 \pm 0.08b	17836.80 \pm 0.09c	236340 \pm 0.09a
M_w (kg/mol)	43156.80 \pm 0.13b	36411.70 \pm 0.23c	50310.70 \pm 0.15a
Polydispersity (M_w/M_n)	2.24 \pm 0.15a	2.04 \pm 0.16a	2.13 \pm 0.18a
Chain length distributions of amylopectin ^f			
ACL (DP)	21.84 \pm 0.48ab	21.32 \pm 0.35b	23.08 \pm 0.85a
f_a ($6 \leq DP \leq 12$) (%)	23.22 \pm 0.98a	24.11 \pm 0.88a	21.35 \pm 0.99a
f_{b1} ($13 \leq DP \leq 24$) (%)	48.49 \pm 0.38ab	49.26 \pm 0.10a	47.29 \pm 0.83b
f_{b2} ($25 \leq DP \leq 36$) (%)	14.85 \pm 0.40ab	14.03 \pm 0.33b	15.26 \pm 0.12a
f_{b3} ($DP \geq 37$) (%)	13.50 \pm 0.10a	12.60 \pm 0.57a	14.07 \pm 1.89a
IR absorbance ratio ^g			
1022/995 cm^{-1}	0.785 \pm 0.020ab	0.759 \pm 0.010b	0.806 \pm 0.010a
1045/1022 cm^{-1}	0.607 \pm 0.003a	0.565 \pm 0.004b	0.606 \pm 0.005a
Relative crystallinity (%)	28.64 \pm 0.98b	26.15 \pm 1.08c	31.31 \pm 0.39a

^a Values in the same column with different lowercase letters are significantly different ($p < 0.05$).

^b L^* , lightness; a^* , redness/greenness; b^* , yellowness/blueness.

^c Granule size is measured by laser diffraction instrument. The d (0.5) is the granule size at which 50% of all the granules by volume are larger. The D [4,3] is the volume-weighted mean diameter.

^d db, dry basis; wb, wet basis.

^e M_n , number-average molecular weight; M_w , weight-average molecular weight.

^f ACL, average chain length of amylopectin; DP, degree of polymerization.

^g IR absorbance ratio is analyzed by using ATR-FTIR.

and Heili starch exhibited a mixture of polyhedral granules with irregular granules that had larger diameters on average. The result was in agreement with the previous reports in different squash varieties (Stevenson et al., 2005). Moreover, scanning electron micrographs showed that Miben starch granules had smooth surface but Heili starch granules displayed some surface indentations, especially in medium-sized granules (Fig. 1). Stevenson et al. (2005) inferred that the surface indentations on squash starch granules were ascribed to non-uniform growth within starch granules or collapse during starch drying.

The granule size distribution of the winter squash and pumpkin starches in aqueous suspensions was determined by the light scattering method. The median diameter of granules, d (0.5), is defined as the diameter for which 50% of particles by volume are larger (Kim, Woo, & Chung, 2018). As shown in Table 1, the d (0.5) of these starches were in the range of 9.51–15.18 μ m. The d (0.5) for Heili starch was the lowest due to its larger portion of smaller granules than Miben and Yinli starch (Fig. 1). Heili starch exhibited the highest specific surface area (0.98 m^2/g) among them (Table 1). Stevenson et al. (2005) calculated the diameter of squash starches by measuring the size of starch granules

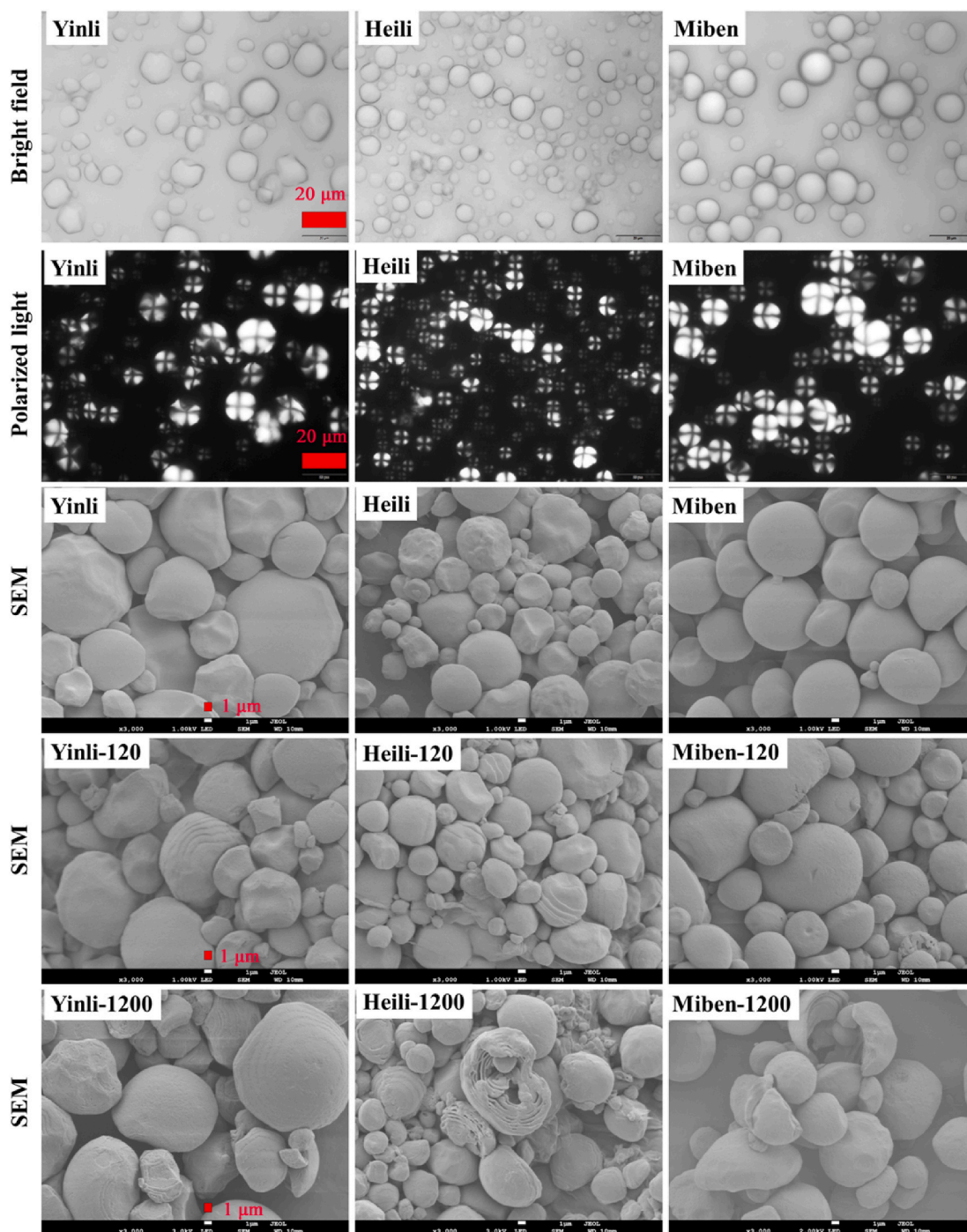


Fig. 1. The morphologies of starch granules under normal light microscope, polarized light microscope, and scanning electron microscope (SEM). 120 and 1200 represented the starch granules had been enzymatically hydrolyzed at 37 °C for 120 min and 1200 min, respectively. Scale bar = 20 μm for optical microphotograph and 1 μm for SEM photograph.

from scanning electron micrographs and found it was ranging from 1.5 to 2.5 μm , 6–8 μm , and 11–13 μm , respectively. Moreover, the volume-weighted mean diameter $D[4, 3]$ of Yinli starch was the largest (45.14 μm), followed by Heili starch (33.10 μm) and Miben starch (21.95 μm). Results showed that the granule size of pumpkin starches significantly varied, depending on cultivars ($p < 0.05$).

3.2. Chemical composition

The starch proximate composition was listed in Table 1. The moisture content of starch samples was found to be 13.36–15.90 g/100 g

(wb). The ash content was 0.19–0.25 g/100 g and showed no significant difference among the samples. The lipid content was 1.01–1.38 g/100 g, which was found to be higher than that reported by Przetaczek-Rożnowska (2017). The protein content of the extracted starches was highest for Miben starch (0.89 g/100 g) but lowest for Yinli starch (0.16 g/100 g), which was comparable to that determined by Przetaczek-Rożnowska (2017). The starch content of the extracted starches was 87.87–92.73 g/100 g.

The apparent amylose content of extracted starch varied significantly ranging from 21.35 g/100 g–30.17 g/100 g. Przetaczek-Rożnowska (2017) observed starches isolated from three pumpkin cultivars grown

in Poland had amylose content of 28.94 g/100 g–32.79 g/100 g. Some other publications reported the apparent amylose content in starches from winter squash (*Cucurbita maxima* D.) and pumpkin (*Cucurbita maxima* var. Ambar) were in the range of 17.43–23.23 g/100 g (Jacek & Izabela, 2016; Stevenson et al., 2005). In this study, Heili and Yinli starches showed significantly higher amylose content than Miben starch ($p < 0.05$). Higher amylose content indicated higher elasticity of starch paste and more susceptibility to retrogradation (Ma, Wang, Wang, Jane, & Du, 2017). Empirical evidence indicated that amylose significantly influence the functional properties of starch. Swarnakar, Srivastav, and Das (2019) suggested that rice with amylose content of 25.11% was suitable for puffing due to its high thermal-induced expansion properties. Reyniers, De Brier, et al. (2020) concluded that the oil uptake of deep-fried potato crisps was dependent on the fine structure of extractable amylose in potato flakes.

3.3. Molecular mass and branch chain length distributions of starches

The elution profiles of winter squash and pumpkin starches (Yinli, Heili and Miben) from the size exclusion chromatography (SEC) column were presented in Fig. 2. The RI chromatograms showed a high molecular weight peak with concentration maxima at the elution time of approximately 40 min, representing the majority of amylopectin populations in each starch sample, whereas the second, low molecular weight peak, with concentration maxima at the elution time of approximately 47 min, which was corresponded largely to amylose populations (You & Izydorczyk, 2002). The average molecular weights of each starch sample were summarized in Table 1. Miben pumpkin starch has M_w of 5.03×10^7 g/mol, which was significantly higher than Yinli and Heili (4.31×10^7 g/mol and 3.64×10^7 g/mol, respectively). Interestingly, the polydispersity values (M_w/M_n) among the winter squash and pumpkin starches (Yinli, Heili and Miben) were not significantly different ($p > 0.05$).

The amylopectin branched chain length distributions of Yinli, Heili and Miben starches were examined after completely debranching by isoamylase and recorded by HPAEC system. The results were compiled and depicted in Fig. 3. The profile of each sample had two peaks. The first peak (strong) was appeared at DP 12 and the second peak (weak) was located at DP 47. As reported by Stevenson et al. (2005), the chromatograms of debranched winter squash amylopectin showed two distinct peaks of short (DP 12–14) and long branch chains. Grouping the degree of polymerization (DP) was conducted according to the classic classification method of Hanashiro, Abe, and Hizukuri (1996), by which the chain length distributions were divided into four parts: f_a ($6 \leq DP \leq 12$), f_{b1} ($13 \leq DP \leq 24$), f_{b2} ($25 \leq DP \leq 36$), f_{b3} ($DP \geq 37$), respectively. As shown in Table 1, all samples had highest portion of f_{b1} and lowest portion of f_{b3} . There was no significant difference between f_a , f_{b1} , f_{b2} ,

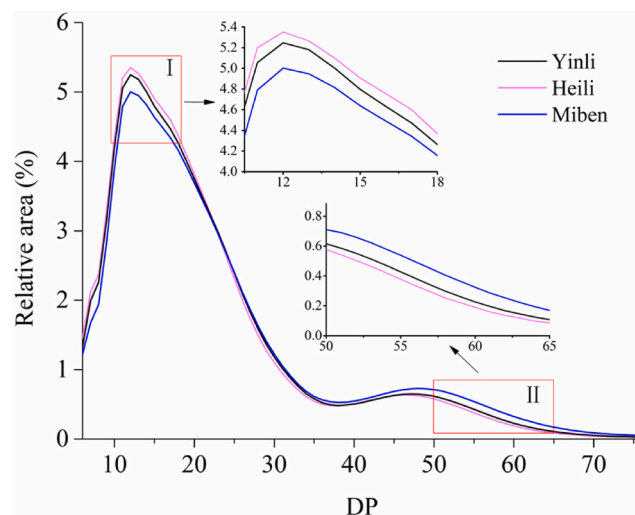


Fig. 3. Profiles of the distribution of amylopectin chain length obtained by high-performance anion-exchange chromatography for Yinli, Heili and Miben starches. DP: degree of polymerization.

and f_{b3} chain length of the winter squash (Yinli and Heili) starches. Similar results were also found for mung bean amylopectin, which the branched chain length distributions for amylopectins from different cultivars showed no statistically significance (Yao et al., 2019). However, the winter squash (Heili) starch has more f_a and f_{b2} chains but less f_{b3} chain, when compared to the pumpkin (Miben) starch. The average chain length (ACL) of these starches was in the range of 21.32–23.08 DP, which was lower than that of winter squashes (*Cucurbita maxima* D.) (26.5–28.1 DP) as reported by Stevenson et al. (2005). Results showed that Miben had the highest ACL value due to more f_{b3} chain for Miben amylopectin.

3.4. Short-range ordered structure and X-ray diffraction pattern of starches

The short-range ordered structure was defined as double-helical order in starch samples (Li et al., 2016). Fig. 4A was representing the deconvoluted ATR-FTIR spectra of the winter squash (Yinli and Heili) and pumpkin (Miben) starches. Absorbance at 1045 cm^{-1} , 1022 cm^{-1} and 995 cm^{-1} from ATR-FTIR spectra were found to be sensitive to starch conformation. The bands at 1045 cm^{-1} and 1022 cm^{-1} were associated with the ordered regions and amorphous regions in starch, respectively (Liu et al., 2021; Sevenou, Hill, Farhat, & Mitchell, 2002). The ratio of absorbance $1045/1022 \text{ cm}^{-1}$ and $1022/995 \text{ cm}^{-1}$ were used to reflect

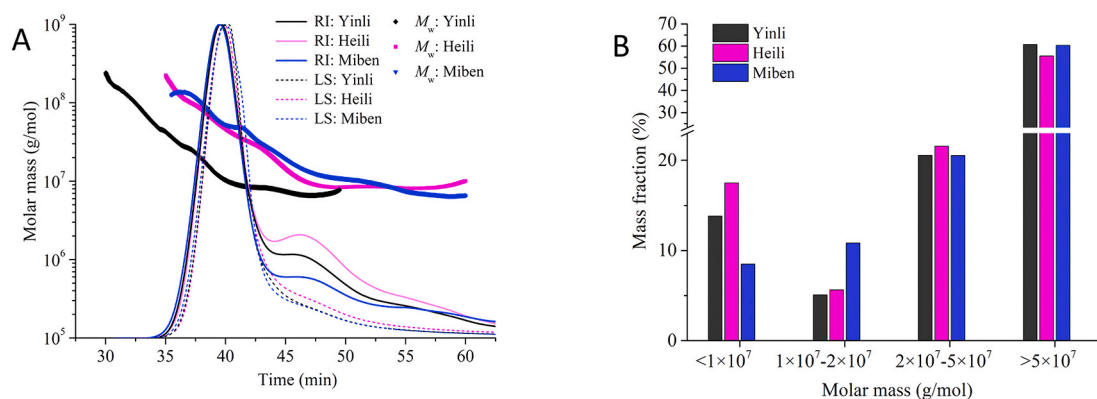


Fig. 2. (A) The profiles of molar mass, light scattering (LS) and refractive index (RI) signals versus elution time (min) of Yinli, Heili and Miben starches produced from refractive index-multi-angle laser light scattering (RI-MALLS) detectors; (B) Cumulative mass fractions at different molecular ranges for Yinli, Heili and Miben starches.

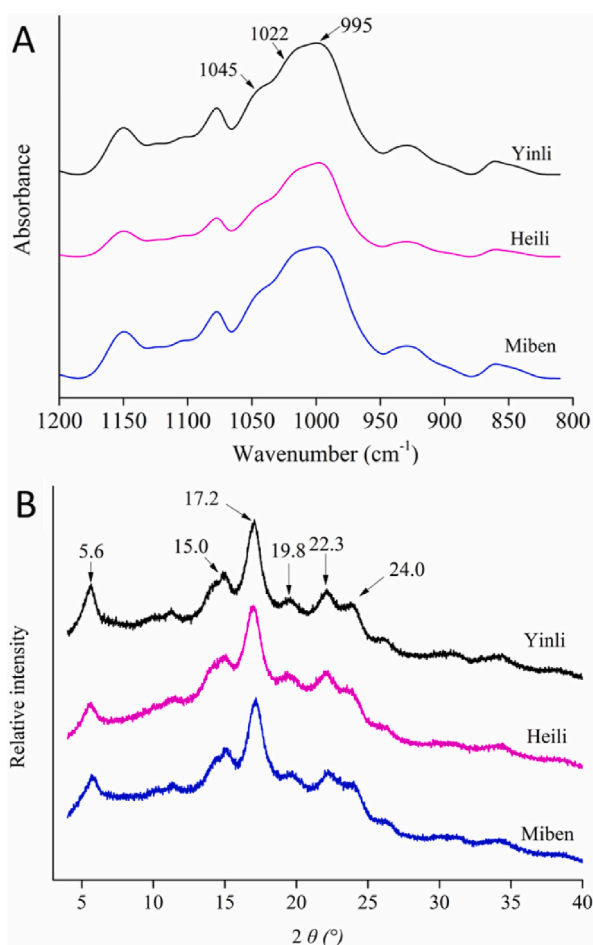


Fig. 4. (A) ATR-FTIR spectra (800–1200 cm⁻¹) and (B) X-ray diffraction patterns of Yinli, Heili and Miben starches.

the degree of order and the ratio of amorphous to ordered structures in the starch granules, respectively (Sevenou et al., 2002). The ratio of absorbance 1045/1022 cm⁻¹ for Heili starch (0.565) was lower than that of Yinli (0.607) and Miben (0.606) starches, which implied that the external (in depth of about 2 μm) region of Heili starch granule was less ordered (Liu et al., 2021).

The X-ray diffractograms of starches isolated from the winter squash and pumpkin fruits were displayed in Fig. 4B, and the degrees of relative crystallinity were shown in Table 1. All starch samples showed a B-type pattern, which had main peaks at $2\theta = 5.6^\circ, 15^\circ, 17.2^\circ, 19.8^\circ, 22.3^\circ$ and 24.0° (Lin et al., 2016). Previous studies showed that starches isolated from pumpkin (*Cucurbita moschata* L.) and winter squash (*Cucurbita maxima* D.) fruit had a characteristic B-type crystalline pattern (Nakhon et al., 2017; Stevenson et al., 2005). Moreover, the small peak at $2\theta = 20.0^\circ$ indicated that the formation of V-type inclusion complexes with lipids in these starches (Lin et al., 2016). Furthermore, Miben starch (31.31%) showed a higher relative crystallinity than Yinli and Heili starches (28.64% and 26.15%). Nakhon et al. (2017) reported that starches isolated from pumpkin (*Cucurbita moschata* L.) had a degree of relative crystallinity 13.35%. However, Stevenson et al. (2005) reported markedly higher degrees of relative crystallinity (ranging from 35% to 55.7%) for starches isolated from seven winter squash cultivars (*Cucurbita maxima* D.) planted at an Iowa State University farm site. Previous studies showed that the starch crystallinity was influenced by amylopectin structure, average amylopectin branch chain length, and amylose content. The degree of relative crystallinity was negative correlated with amylose content, and positive correlated with amylopectin long chain content (Cheetham & Tao, 1998; Lin et al., 2016).

Amylopectin long branch chains were prone to form double helices and pack together into crystallites, which could be responsible for the degree of crystallinity (Li et al., 2020). In this context, the higher relative crystallinity of Miben starch could be contributed to its lower amylose content (reversely higher amylopectin content) and higher ACL value of amylopectin populations.

3.5. Lamellar and fractal structure of starches

Small-angle X-ray scattering (SAXS) technique was applied to evaluate the semi-crystalline lamellar structure of starches isolated from winter squash and pumpkin fruits. Fig. 5 presented the double logarithmic SAXS patterns of the native and enzymatically hydrolyzed starch samples. It was clearly seen that one scattering peak was located in $0.635\text{--}0.655\text{ nm}^{-1}$. According to the Woolf-Bragg's equation $D_{\text{Bragg}} = 2\pi/q$, there is a 9–10 nm period structure in the starch samples. The D_{Bragg} of Yinli, Heili and Miben starches was ca. 9.80 nm, 9.71 nm, and 9.59 nm, respectively (Table 2), suggesting that Yinli possessed thicker semi-crystalline lamellae than the others (Liu et al., 2021). It was also found that the scattering intensity of Yinli starch was the strongest among them. The higher scattering intensity of Yinli starch was probably related to the higher electron density contrast between crystalline and amorphous lamellae (Lan et al., 2016; Suzuki, Chiba, & Yarmo, 1997). In addition, the peak width at half maximum of the scattering peak was related to the poly-dispersity of the crystalline-amorphous lamellae (Witt, Douch, Gilbert, & Gilbert, 2012). In this context, Heili starch displayed a narrower peak, indicating the existence of relatively less polydispersed semi-crystalline lamellae in Heili starch. After 1200 min enzymatic hydrolysis, the D_{Bragg} for each digested starch increased by 0.093 nm (Yinli), 0.091 nm (Heili) and 0.163 nm (Miben), respectively. This was probably due to the movement of double helices during the digestion by inducing the disorganization of starch semi-crystalline structure (Liu et al., 2021). Furthermore, the enzymatic hydrolysis markedly reduced the visibility of the scattering peak of Heili starch, implying an obvious decrease in the ordering degree of semi-crystalline lamellae (Lan et al., 2016). The enzymatic amylolysis aggravating the stacking disorder was frequently concluded in the previous studies (Lan et al., 2016).

In theory, the scattering pattern from a fractal object generally obeys the power law (Suzuki et al., 1997)

$$I \propto q^{-\alpha} \quad (1)$$

Where I is the scattering intensity, and q is the scattering vector. The

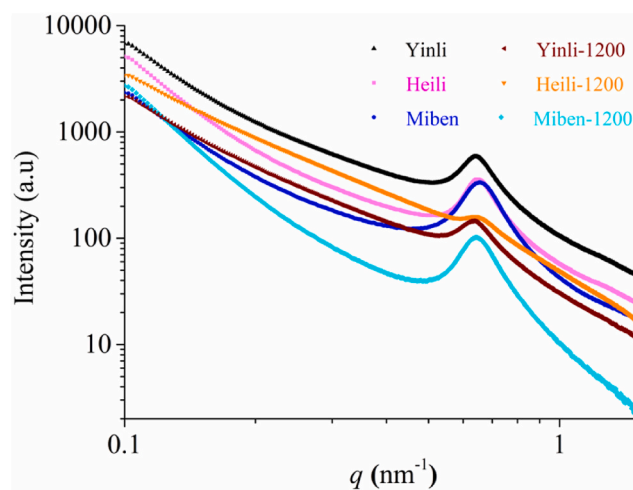


Fig. 5. Double logarithmic SAXS patterns of native starches (Yinli, Heili and Miben) and starches (Yinli-1200, Heili-1200 and Miben-1200) enzymatically hydrolyzed at 37 °C for 1200 min.

Table 2
SAXS characteristics of native and enzymatically hydrolyzed starch granules ^a.

Starch samples ^b	Peak intensity (a.u)	Peak position (nm ⁻¹)	Peak width at half maximum (nm ⁻¹)	D_{Bragg} (nm)	α	D_s	D_m
Yinli	164.380	0.641	0.121	9.802	-2.006	-	2.006
Heili	116.438	0.647	0.098	9.711	-2.347	-	2.347
Miben	119.860	0.655	0.128	9.593	-2.119	-	2.119
Yinli-1200	30.820	0.635	0.121	9.895	-1.962	-	1.962
Heili-1200	13.699	0.641	0.068	9.802	-1.845	-	1.845
Miben-1200	37.671	0.644	0.132	9.756	-3.010	2.990	-

^a D_{Bragg} means the Bragg spacing; α means the characteristic parameter related to the fractal dimension; D_s means the surface fractal dimension; D_m means the mass fractal dimension.

^b 1200 means the starches had been enzymatically hydrolyzed for 1200 min.

exponent α ($-4 < \alpha < -1$) is the characteristic parameter related to the fractal dimension.

The values of α and D_m can be calculated by Eq. (2):

$$\ln I(q) = \ln I_0 - \alpha \ln q \quad (2)$$

When $-4 < \alpha < -3$, the scattering can be judged as reflection from the surface or interface, which is classified as “surface fractal”. The surface fractal dimension D_s can be calculated by Eq. (3):

$$D_s = 6 + \alpha \quad (3)$$

When $-3 < \alpha < -1$, the scattering can be classified as “mass fractal”. The mass fractal dimension D_m can be calculated by Eq. (4):

$$D_m = -\alpha \quad (4)$$

In this work, the SAXS parameters were shown in Table 2. It was found that α of untreated starches took the range from -3 to -1 , so that these starches can be classified as “mass fractal”. The mass fractal dimension of Heili pumpkin starch was the largest, indicating that the mass of the scattering objects is the highest degree of compactness (Suzuki et al., 1997). After 1200 min enzymatically hydrolysis, Yinli and Heilin starches still showed mass fractal dimension ($-3 < \alpha < -1$). However, digested Miben pumpkin starch showed surface fractal dimension due to $\alpha < -3$.

3.6. Thermal and pasting properties

The thermal characteristics of winter squash and pumpkin starches were measured by DSC. The heat flow curves of the pumpkin starches were shown in Fig. 6A. The thermal parameters (T_o , T_p , T_c , and ΔT) and the enthalpy change (ΔH) were summarized in Table 3. The thermal parameters including onset ($T_o = 61.31$ – 66.87 °C), peak ($T_p = 64.82$ – 71.56 °C) and conclusion ($T_c = 71.02$ – 78.02 °C) temperatures for Yinli, Heili and Miben starches were in accordance with the values for starches isolated from three types of pumpkin fruits (*Cucurbita maxima*) as reported by Przetaczek-Rożnowska (2017). Moreover, Heili starch had significantly lower onset ($T_o = 61.31$ °C) and peak ($T_p = 61.31$ °C) gelatinization temperatures than Yinli and Miben starches. Miben starch gelatinized over the widest temperature range ($\Delta T = T_c - T_o = 11.15$ °C), followed by Heili (9.7 °C) and Yinli (8.52 °C). The enthalpy change (ΔH) of Heili starch (10.43 J/g) was also lower than that of Yinli and Miben starches (13.92 and 16.89 J/g). The gelatinization of starch has been found to be influenced by interactive factors including granule morphology, amylose/amylopectin ratio, structures of starch molecules, and minor-component of contents. Heili starch had the smallest granule size among these starches (Table 1). To some extent, the gelatinization enthalpy change was positive related to the granules size of the starch from the same biological origin. According to Liu et al. (2017), the large-size rice starch granule was significantly higher in the levels of T_p and ΔH than the small-size one, regardless of rice genotype. Moreover, Heili starch had the smallest molecular mass, higher specific surface area of granules, lowest degree of short-range order, lower average chain length and larger amount of short chains ($DP < 12$). These

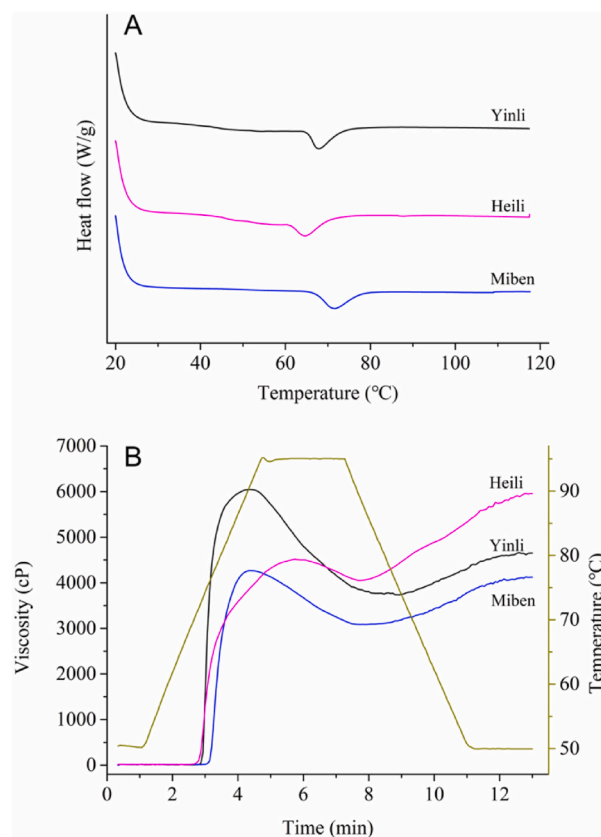


Fig. 6. DSC thermograms (A), and RVA profiles (B) of Yinli, Heili and Miben starches.

characteristics could be attributed to the lower gelatinization temperatures and enthalpy change (Noda et al., 2004; Singh, Singh, Isono, & Noda, 2010). Miben starch had the highest degree of relative crystallinity (31.31%) and largest molecular mass (5.03×10^7 g/mol), which might be closely related to its highest onset ($T_o = 66.87$ °C) and peak ($T_p = 71.56$ °C) gelatinization temperatures. As reported by Singh et al. (2010), the structures of amylopectin could be responsible to the thermal properties. They concluded that the gelatinization enthalpy change was negatively correlated with short length chains of amylopectin and positively correlated with medium length chains of amylopectin. In our study, Miben starch had larger amount of f_{b2} and smaller amount of f_a (Fig. 3), which could be ascribed to higher enthalpy change (16.89 J/g).

The pasting profiles of winter squash and pumpkin starches were depicted in Fig. 6B and the pasting parameters were summarized in Table 3. As shown in Fig. 6B, the pasting curves showed significant variation among Yinli, Heili and Miben starches. All starch samples contained similar lipid and ash contents (Table 1). Therefore, the differences in pasting properties among them were unlikely due to the lipid

Table 3
Thermal and pasting properties of starches from winter squash and pumpkin ^a.

Parameters	Cultivars		
	Yinli	Heili	Miben
Thermal properties ^b			
T_o (°C)	65.26 ± 0.14b	61.31 ± 0.08c	66.87 ± 0.29a
T_p (°C)	67.89 ± 0.14b	64.82 ± 0.19c	71.56 ± 0.27a
T_c (°C)	73.78 ± 0.46b	71.02 ± 0.17c	78.02 ± 0.36a
ΔT (°C)	8.52 ± 0.44c	9.70 ± 0.09b	11.15 ± 0.11a
ΔH (J/g)	13.92 ± 0.88ab	10.43 ± 1.32b	16.89 ± 3.09a
Pasting properties ^c			
PT (°C)	72.28 ± 0.38b	70.63 ± 0.53c	75.15 ± 0.07a
TTPV (min)	4.33 ± 0.0b	5.83 ± 0.1a	4.40 ± 0.0b
PV (cP)	6266 ± 219.00a	4689.5 ± 243.95b	4468 ± 284.26b
TV (cP)	3876.5 ± 140.5a	4259.5 ± 290.62a	3116 ± 42.43b
BD (cP)	2389.5 ± 78.5a	430 ± 46.67c	1352 ± 241.83b
FV (cP)	4663.5 ± 13.5b	6073 ± 164.05a	4075 ± 67.88b
SB (cP)	787.0 ± 127.0c	1813.5 ± 126.57a	959 ± 110.31b

^a Values were means ± standard deviations, n = 3. Values within the same row with different lowercase letters are significantly different ($p < 0.05$).

^b T_o , T_p , and T_c represent onset, peak, and completion gelatinization temperatures, respectively. ΔT means the difference between T_o and T_c ; ΔH , gelatinization enthalpies.

^c PT, TTPV, PV, TV, BD, FV and SB mean pasting temperature, time to peak viscosity, pasting viscosity, trough viscosity, breakdown viscosity, final viscosity and setback viscosity.

and ash contents. Pasting temperature (PT) i.e., the temperature at which the starch granules began to swell varied from 70.63 °C (Heili) to 75.15 °C (Miben). This reveals that the long- and short-range ordered molecular structures of Heili starch were easier ruptured than others (Wang et al., 2021), which was consistent with the lowest T_o as measured by DSC (Fig. 6A). Upon heating, the increase of viscosity for starch-water system was mainly correlated with the swelling of starch granules and amylose leaching from the granules (Malumba et al., 2017). Similar time to peak viscosity (TTPV) was found in Yinli (4.33 min) and Miben (4.40 min) starches. However, Heili starch took more time (5.83 min) to reach peak viscosity, indicating the lowest rate at which the granules reached maximum swelling. In addition, Yinli starch had highest peak viscosity (PV), which was probably due to excellent swelling capacity and resistance to rupture. Once peak viscosity had been reached, a decrease in viscosity started for the winter squash and pumpkin starch samples, which was mainly due to the disintegration of swollen starch granules under shearing with continual heating (Xie et al., 2006). Breakdown viscosity (BD) measured the disintegration degree of swollen starch granules upon shear and heat. As shown in Table 3, the lowest BD was found in Heili starch (430 cP) and the highest in Yinli starch (2389.5 cP). Final viscosity (FV) reflected the thickening capacity of starch pastes (Guo et al., 2019). FV of starches from all cultivars increased upon cooling, with Heili starch (6073 cP) exhibiting significantly highest final viscosity than others. Setback viscosity (SB) measured as the difference between TV and FV. SB represents the increase in viscosity during the cooling period resulting from the rearrangement of starch molecules, especially leached amylose in the continuous phase (Huang et al., 2015). Heili starch displayed much higher setback viscosity than Yinli and Miben, indicating that Heili starch had stronger tendency to retrograde (Zhang, Chen, Li, & Zhang, 2015). As shown in Fig. 2B, the mass fraction of $M_w < 1 \times 10^7$ g/mol was mainly designated as amylose population (Li, Wen, Wang, & Sun, 2018). The mass fraction of this part for Heili starch was markedly higher than Yinli and Miben starches, which was contributed to the short-term retrogradation of starch paste.

3.7. Enzymatic hydrolysis properties of starch

The time course of starch hydrolysis was charted in Fig. 7. The hydrolysis displayed a biphasic trend i.e., a relatively high rate at the initial

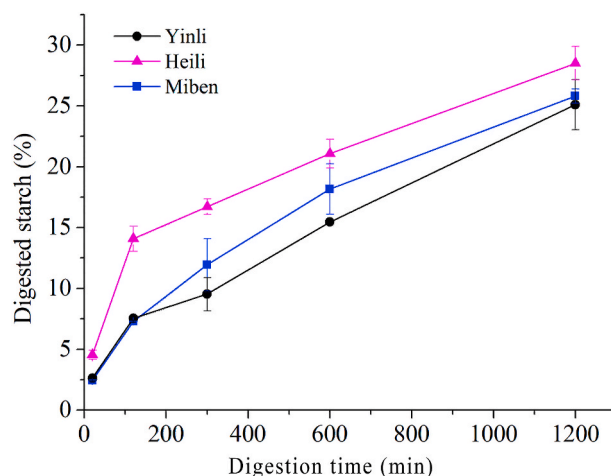


Fig. 7. The dynamic curves of *in vitro* enzymatic digestion of Yinli, Heili and Miben starch granules.

stage following with a progressively decreased rate thereafter (Huang et al., 2015). After hydrolyzed for 1200 min, the proportion of digested Heili starch was approximately 28%, while that of Miben and Yinli starches was about 25%. The higher digested ratio for Heili starch was probably related to its lower crystallinity and smaller particle size (Benmoussa, Moldenhauer, & Hamaker, 2007) as well as higher proportion of short-chain amylopectin (Bertoft et al., 2016).

The SEM images of winter squash and pumpkin starch granules in their native state and after *in vitro* digestion with α -amylase and glucosidase for 120 min and extended time (up to 1200 min) at 37 °C were given in Fig. 1. It was observed that the starch granules were eroded by the enzymes. For all samples, the formation of holes did not occurred during the amylolysis. Instead, a layered structure of growth rings was exhibited for two winter squash starches, while damaged or fragmented regions were also showed in pumpkin starch granules. The layered structure of growth rings, as seen in digested Yinli and Heili starches, were probably due to a gradient in packing density of starch molecules related to the photosynthetically controlled supply of starch precursor (Malumba et al., 2017).

3.8. *In vitro* starch digestibility

The enzymatic hydrolysis of native, gelatinized and retrograded starches was performed, respectively. The results were listed in Table 4. The hydrolysis of native starches was limited, for the RDS contents for all starches were less than 5%. These results were ascribed to the intact granules with concentrically arranged starch molecules, resulting in high resistance to digestion (Ma et al., 2017). However, the gelatinized starches underwent disorganization of their structure, thereby much susceptible to enzymatic hydrolysis. The RDS contents of gelatinized starches markedly increased to 78.13%, 84.23% and 90.53% for Miben, Yinli and Heili, respectively. Interestingly, gelatinized winter squash and pumpkin starches had higher amount of RS (8.20–18.79%) than SDS (1.27–4.13%). This result could be explained by the following reasons. Firstly, the starch digestibility was strongly depended the accessibility of starch chains to the amylolytic enzymes or the capability of starch-enzyme binding. The gelatinized starch could be considered as a combination of dispersed starch molecules and starch fragments. Juan-sang, Puttanlek, Rungsardthong, Pancha-arnon, and Uttapap (2012) claimed that the level of starch granule disintegration played an important role on the SDS and RS fraction of canna starches in gelatinized state, which the gelatinization was performed at 100 °C on a rapid visco analyzer. Secondly, the starch digestibility was affected by the molecular structure and arrangement. Zhang et al. (2018) reported that the gelatinized starches from seven purple sweet potato cultivars

Table 4
Digestion properties of native, gelatinized and retrograded starches. ^a

Cultivars	Native starch			Gelatinized starch			Retrograded starch		
	RDS (%) ^b	SDS (%) ^b	RS (%) ^b	RDS (%)	SDS (%)	RS (%)	RDS (%)	SDS (%)	RS (%)
YinLi	2.63 ± 0.05b	4.91 ± 0.22b	92.76 ± 2.22a	84.23 ± 0.54b	4.13 ± 1.26a	11.64 ± 1.75b	73.15 ± 0.34b	6.69 ± 0.03b	20.16 ± 0.31a
HeiLi	4.54 ± 0.35a	9.56 ± 1.11a	85.90 ± 1.47b	90.53 ± 0.66a	1.27 ± 0.60b	8.20 ± 0.48c	77.84 ± 1.05a	10.33 ± 1.10a	11.83 ± 1.95b
Miben	2.45 ± 0.04b	4.84 ± 2.16b	92.71 ± 0.27a	78.13 ± 0.73b	3.07 ± 0.40a	18.79 ± 1.13a	74.27 ± 0.62b	6.43 ± 1.02b	19.30 ± 1.97a

^a Values were means ± standard deviations, n = 3. Values in the same column with different lowercase letters are significantly different ($p < 0.05$).

^b RDS, rapidly digestible starch; SDS, slowly digestible starch; RS, resistant starch.

contained comparably more RS than SDS. Similarly, [Bian and Chung \(2016\)](#) reported that the native and modified rice starches in their gelatinized state showed higher RS content than SDS content. This was explained as the interaction between amylose and amylose chains restricting the accessibility of starch chains to the amylolytic enzymes ([Bian & Chung, 2016](#)). As expected, the RS content of retrograded starches was higher than that of gelatinized ones. The increase in RS content may be attributed to recrystallization of starch molecules into double helices that forming tightly packed structures ([Zhu & Liu, 2020](#)).

4. Conclusion

Starches were extracted from winter squash and pumpkin fruits. They all displayed a mixture of polyhedral and spherical granules, but showed significant difference in granular size. All starches exhibited B-type crystallinity, but had some differences in relative crystallinity, amylose content, molecular weight and amylopectin branch chain distribution, thermal properties, pasting properties, and enzymatic hydrolysis properties. The amylose content was higher in starches from winter squash (Yinli and Heili) than that from pumpkin (Miben). Heili starch had the lowest granular size, lowest degree of short-range order, highest mass fraction of $<1 \times 10^7$ g/mol starch molecule populations. The gelatinization temperature (T_o , T_p , and T_c) and the enthalpy change (ΔH) was the lowest in Heili starch and the highest in Miben starch. Heili starch took more time to reach the peak viscosity and had the highest final and setback viscosities. The highest peak viscosity and the lowest setback viscosity were found in Yinli starch. All the starch granules showed high resistance to *in vitro* digestion. Among them, the erosion of granule surface and destruction of ordered structures (semi-crystalline lamellae) was more evidently induced in Heili starch, as suggested by scanning electron microscopy (SEM) and small angle X-ray scattering (SAXS). The gelatinized and retrograded Yinli and Miben starches had comparable SDS content. However, the SDS and RS contents were found the lowest in gelatinized and retrograded Heili starch.

We expect that the results of this study could provide useful information for the further utilization of starches from winter squash and pumpkin in food and nonfood industries such as thickeners, stabilizers or bio-plastic packaging. In addition, our results suggest that the winter squash and pumpkin starches presented a good source of resistant starch, compared with green banana flour and potato starch powder which are already being used commercially for prebiotic or nutritional supplements.

Author statement

Tiantian Yuan: Methodology, Investigation, Visualization, Writing – original draft. Fayin Ye: Conceptualization, Methodology, Formal analysis, Writing – review & editing. Ting Chen: Methodology, Formal analysis. Mengsa Li: Methodology, Formal analysis. Guohua Zhao: Formal analysis, Writing – review & editing.

Declaration of competing interest

The authors declared that they have no conflicts of interest to this work. We declare that we do not have any commercial or associative

interest that represents a conflict of interest in connection with the work submitted.

Acknowledgements

This research was funded by the National Natural Science Foundation of China (31871837 and 31601401). The authors thank 1W2A SAXS station at the Beijing Synchrotron Radiation Facility (BSRF) for courteously supporting the SAXS analysis.

References

- Al-Ghamdi, S., Hong, Y.-K., Qu, Z., & Sablani, S. S. (2020). State diagram, water sorption isotherms and color stability of pumpkin (*Cucurbita pepo* L.). *Journal of Food Engineering*, 273, Article 109820. <https://doi.org/10.1016/j.jfoodeng.2019.109820>
- AOAC. (2000). In *Official method of analysis* (17th ed.). Gaithersburg, MD: Association of Official Analytical Chemists.
- AOAC. (2006). In *Official methods of analysis* (15th ed.). Washington DC: Association of Official Analytical Chemists.
- Bai, Y., Zhang, M., Chandra Atluri, S., Chen, J., & Gilbert, R. G. (2020). Relations between digestibility and structures of pumpkin starches and pectins. *Food Hydrocolloids*, 106, Article 105894. <https://doi.org/10.1016/j.foodhyd.2020.105894>
- Benmoussa, M., Moldenhauer, K. A. K., & Hamaker, B. R. (2007). Rice amylopectin fine structure variability affects starch digestion properties. *Journal of Agricultural and Food Chemistry*, 55(4), 1475–1479. <https://doi.org/10.1021/jf062349x>
- Bertoft, E., Annor, G. A., Shen, X., Rumpagaporn, P., Seetharaman, K., & Hamaker, B. R. (2016). Small differences in amylopectin fine structure may explain large functional differences of starch. *Carbohydrate Polymers*, 140(20), 113–121. <https://doi.org/10.1016/j.carbpol.2015.12.025>
- Bian, L., & Chung, H.-J. (2016). Molecular structure and physicochemical properties of starch isolated from hydrothermally treated brown rice flour. *Food Hydrocolloids*, 60, 345–352. <https://doi.org/10.1016/j.foodhyd.2016.04.008>
- Cheatham, N. W. H., & Tao, L. (1998). Variation in crystalline type with amylose content in maize starch granules: An X-ray powder diffraction study. *Carbohydrate Polymers*, 36(4), 277–284. [https://doi.org/10.1016/S0144-8617\(98\)00007-1](https://doi.org/10.1016/S0144-8617(98)00007-1)
- Chen, Y.-F., Singh, J., & Archer, R. (2018). Potato starch retrogradation in tuber: Structural changes and gastro-small intestinal digestion *in vitro*. *Food Hydrocolloids*, 84, 552–560. <https://doi.org/10.1016/j.foodhyd.2018.05.044>
- Corrigan, V. K., Hurst, P. L., & Potter, J. F. (2001). Winter squash (*Cucurbita maxima*) texture: Sensory, chemical, and physical measures. *New Zealand Journal of Crop and Horticultural Science*, 29(2), 111–124. <https://doi.org/10.1080/01140671.2001.9514169>
- Englyst, H., Kingman, S., & Cummings, J. (1992). Classification and measurement of nutritionally important starch fractions. *European Journal of Clinical Nutrition*, 46 (Suppl. 2), S33–S50.
- Guo, K., Liu, T., Xu, A., Zhang, L., Bian, X., & Wei, C. (2019). Structural and functional properties of starches from root tubers of white, yellow, and purple sweet potatoes. *Food Hydrocolloids*, 89, 829–836. <https://doi.org/10.1016/j.foodhyd.2018.11.058>
- Hanashiro, I., Abe, J.-i., & Hizukuri, S. (1996). A periodic distribution of the chain length of amylopectin as revealed by high-performance anion-exchange chromatography. *Carbohydrate Research*, 283, 151–159. [https://doi.org/10.1016/0008-6215\(95\)00408-4](https://doi.org/10.1016/0008-6215(95)00408-4)
- Hu, Y., Li, C., Regenstein, J. M., & Wang, L. (2019). Preparation and properties of potato amylose-based fat replacer using super-heated quenching. *Carbohydrate Polymers*, 223, Article 115020. <https://doi.org/10.1016/j.carbpol.2019.115020>
- Huang, J., Zhao, L., Huai, H., Li, E., Zhang, F., & Wei, C. (2015). Structural and functional properties of starches from wild *Trapa quadrispinosa*, *jaпонica*, *mammillifera* and *incisa*. *Food Hydrocolloids*, 48, 117–126. <https://doi.org/10.1016/j.foodhyd.2015.02.003>
- Hurst, P. L., Corrigan, V. K., Hannan, P. J., & Lill, R. E. (1995). Storage rots, compositional analysis, and sensory quality of three cultivars of butternut squash. *New Zealand Journal of Crop and Horticultural Science*, 23(1), 89–95. <https://doi.org/10.1080/01140671.1995.9513872>
- Jacek, R., & Izabela, P. R. (2016). Physicochemical properties of native and phosphorylated pumpkin starch. *Starch - Stärke*, 69(1–2), Article 1500358. <https://doi.org/10.1002/star.201500358>

- Juansang, J., Puttanlek, C., Rungsardthong, V., Pancha-arnon, S., & Uttapap, D. (2012). Effect of gelatinisation on slowly digestible starch and resistant starch of heat-moisture treated and chemically modified canna starches. *Food Chemistry*, 131(2), 500–507. <https://doi.org/10.1016/j.foodchem.2011.09.013>
- Jun, H.-I., Lee, C.-H., Song, G.-S., & Kim, Y.-S. (2006). Characterization of the pectic polysaccharides from pumpkin peel. *Lebensmittel-Wissenschaft und -Technologie: Food Science and Technology*, 39(5), 554–561. <https://doi.org/10.1016/j.lwt.2005.03.004>
- Kim, Y.-y., Woo, K. S., & Chung, H.-J. (2018). Starch characteristics of cowpea and mungbean cultivars grown in Korea. *Food Chemistry*, 263, 104–111. <https://doi.org/10.1016/j.foodchem.2018.04.114>
- Lan, X., Xie, S., Wu, J., Xie, F., Liu, X., & Wang, Z. (2016). Thermal and enzymatic degradation induced ultrastructure changes in canna starch: Further insights into short-range and long-range structural orders. *Food Hydrocolloids*, 58, 335–342. <https://doi.org/10.1016/j.foodhyd.2016.02.018>
- Li, Y., Liu, H., Wang, Y., Shabani, K. I., Qin, X., & Liu, X. (2020). Comparison of structural features of reconstituted doughs affected by starches from different cereals and other botanical sources. *Journal of Cereal Science*, 93, Article 102937. <https://doi.org/10.1016/j.jcs.2020.102937>
- Lin, L., Guo, D., Zhao, L., Zhang, X., Wang, J., Zhang, F., et al. (2016). Comparative structure of starches from high-amylose maize inbred lines and their hybrids. *Food Hydrocolloids*, 52, 19–28. <https://doi.org/10.1016/j.foodhyd.2015.06.008>
- Liu, C., Jiang, Y., Liu, J., Li, K., & Li, J. (2021). Insights into the multiscale structure and pasting properties of ball-milled waxy maize and waxy rice starches. *International Journal of Biological Macromolecules*, 168, 205–214. <https://doi.org/10.1016/j.ijbiomac.2020.12.048>
- Liu, J., Zhao, Q., Zhou, L., Cao, Z., Shi, C., & Cheng, F. (2017). Influence of environmental temperature during grain filling period on granule size distribution of rice starch and its relation to gelatinization properties. *Journal of Cereal Science*, 76, 42–55. <https://doi.org/10.1016/j.jcs.2017.05.004>
- Li, H., Wen, Y., Wang, J., & Sun, B. (2018). Relations between chain-length distribution, molecular size, and amylose content of rice starches. *International Journal of Biological Macromolecules*, 120, 2017–2025. <https://doi.org/10.1016/j.ijbiomac.2018.09.204>
- Malumba, P., Doran, L., Zanmenou, W., Odjo, S., Katanga, J., Blecker, C., et al. (2017). Morphological, structural and functional properties of starch granules extracted from the tubers and seeds of *Sphenostylis stenocarpa*. *Carbohydrate Polymers*, 178, 286–294. <https://doi.org/10.1016/j.carbpol.2017.09.013>
- Ma, M., Wang, Y., Wang, M., Jane, J.-L., & Du, S.-k. (2017). Physicochemical properties and *in vitro* digestibility of legume starches. *Food Hydrocolloids*, 63, 249–255. <https://doi.org/10.1016/j.foodhyd.2016.09.004>
- Nakhon, P. P. S., Jangchud, K., Jangchud, A., & Prinyawiwatkul, W. (2017). Comparisons of physicochemical properties and antioxidant activities among pumpkin (*Cucurbita moschata* L.) flour and isolated starches from fresh pumpkin or flour. *International Journal of Food Science and Technology*, 52(11), 2436–2444. <https://doi.org/10.1111/ijfs.13528>
- Noda, T., Tsuda, S., Mori, M., Takigawa, S., Matsuura-Endo, C., Saito, K., et al. (2004). The effect of harvest dates on the starch properties of various potato cultivars. *Food Chemistry*, 86(1), 119–125. <https://doi.org/10.1016/j.foodchem.2003.09.035>
- Przetaczek-Rożnowska, I. (2017). Physicochemical properties of starches isolated from pumpkin compared with potato and corn starches. *International Journal of Biological Macromolecules*, 101, 536–542. <https://doi.org/10.1016/j.ijbiomac.2017.03.092>
- Qiao, D., Tu, W., Liao, A., Li, N., Zhang, B., Jiang, F., et al. (2019). Multi-scale structure and pasting/digestion features of yam bean tuber starches. *Carbohydrate Polymers*, 213, 199–207. <https://doi.org/10.1016/j.carbpol.2019.02.082>
- Reyniers, S., Vluymans, N., De Brier, N., Ooms, N., Matthijs, S., Brijs, K., et al. (2020a). Amylolysis as a tool to control amylose chain length and to tailor gel formation during potato-based crisp making. *Food Hydrocolloids*, 103, Article 105658. <https://doi.org/10.1016/j.foodhyd.2020.105658>
- Reyniers, S., De Brier, N., Ooms, N., Matthijs, S., Piovesan, A., Verboven, P., Brijs, K., Gilbert, R. G., & Delcour, J. A. (2020b). Amylose molecular fine structure dictates water-oil dynamics during deep-frying and the calorific density of potato crisps. *Nature Food*, 1(11), 736–745. <http://orcid.org/0000-0003-2954-1022>
- Rezig, L., Chibani, F., Chouaibi, M., Dalgalarondo, M., Hessini, K., Guéguen, J., et al. (2013). Pumpkin (*Cucurbita maxima*) seed proteins: Sequential extraction processing and fraction characterization. *Journal of Agricultural and Food Chemistry*, 61(32), 7715–7721. <https://doi.org/10.1021/jf402323u>
- Rolnik, A., & Olas, B. (2020). Vegetables from the Cucurbitaceae family and their products: Positive effect on human health. *Nutrition*, 78, Article 110788. <https://doi.org/10.1016/j.nut.2020.110788>
- Rożnowski, J., Przetaczek-Rożnowska, I., & Boba, D. (2016). Physicochemical properties of native and phosphorylated pumpkin starch. *Starch - Stärke*, 69, Article 1500358. <https://doi.org/10.1002/star.201500358>
- Sevenou, O., Hill, S. E., Farhat, I. A., & Mitchell, J. R. (2002). Organisation of the external region of the starch granule as determined by infrared spectroscopy. *International Journal of Biological Macromolecules*, 31(1), 79–85. [https://doi.org/10.1016/S0141-8130\(02\)00067-3](https://doi.org/10.1016/S0141-8130(02)00067-3)
- Singh, S., Singh, N., Isono, N., & Noda, T. (2010). Relationship of granule size distribution and amylopectin structure with pasting, thermal, and retrogradation properties in wheat starch. *Journal of Agricultural and Food Chemistry*, 58, 1180–1188. <https://doi.org/10.1021/jf902753f>
- Stevenson, D. G., Yoo, S.-H., Hurst, P. L., & Jane, J.-I. (2005). Structural and physicochemical characteristics of winter squash (*Cucurbita maxima* D.) fruit starches at harvest. *Carbohydrate Polymers*, 59(2), 153–163. <https://doi.org/10.1016/j.carbpol.2004.08.030>
- Suzuki, T., Chiba, A., & Yarno, T. (1997). Interpretation of small angle X-ray scattering from starch on the basis of fractals. *Carbohydrate Polymers*, 34(4), 357–363. [https://doi.org/10.1016/S0144-8617\(97\)00170-7](https://doi.org/10.1016/S0144-8617(97)00170-7)
- Swarnakar, A., Srivastav, P., & Das, S. K. (2019). Optimization of preconditioning process of pressure parboiled brown rice (unpolished) for microwave puffing and its comparison with hot sand bed puffing. *Journal of Food Process Engineering*, 42, Article 13007. <https://doi.org/10.1111/jfpe.13007>
- Wang, H., Xu, K., Liu, X., Zhang, Y., Xie, X., & Zhang, H. (2021). Understanding the structural, pasting and digestion properties of starch isolated from frozen wheat dough. *Food Hydrocolloids*, 111, Article 106168. <https://doi.org/10.1016/j.foodhyd.2020.106168>
- Witt, T., Douth, J., Gilbert, E. P., & Gilbert, R. G. (2012). Relations between molecular, crystalline, and lamellar structures of amylopectin. *Biomacromolecules*, 13(12), 4273–4282. <https://doi.org/10.1021/bm301586x>
- Xie, F., Liu, H., Chen, P., Xue, T., Chen, L., Yu, L., et al. (2006). Starch gelatinization under shearless and shear conditions. *International Journal of Food Engineering*, 2(5), Article 6. <https://doi.org/10.2202/1556-3758.1162>
- Yao, M., Tian, Y., Yang, W., Huang, M., Zhou, S., & Liu, X. (2019). The multi-scale structure, thermal and digestion properties of mung bean starch. *International Journal of Biological Macromolecules*, 131, 871–878. <https://doi.org/10.1016/j.ijbiomac.2019.03.102>
- You, S., & Izydorczyk, M. S. (2002). Molecular characteristics of barley starches with variable amylose content. *Carbohydrate Polymers*, 49(1), 33–42. [https://doi.org/10.1016/S0144-8617\(01\)00300-9](https://doi.org/10.1016/S0144-8617(01)00300-9)
- Zabot, G. L., Silva, E. K., Emerick, L. B., Felisberto, M., & Meireles, M. (2018). Physicochemical, morphological, thermal and pasting properties of a novel native starch obtained from annatto seeds. *Food Hydrocolloids*, 89, 321–329. <https://doi.org/10.1016/j.foodhyd.2018.10.041>
- Zhang, B., Chen, L., Li, X., Li, L., & Zhang, H. (2015). Understanding the multi-scale structure and functional properties of starch modulated by glow-plasma: A structure-functionality relationship. *Food Hydrocolloids*, 50, 228–236. <https://doi.org/10.1016/j.foodhyd.2015.05.002>
- Zhang, B., Li, X., Liu, J., Xie, F., & Chen, L. (2013). Supramolecular structure of A- and B-type granules of wheat starch. *Food Hydrocolloids*, 31(1), 68–73. <https://doi.org/10.1016/j.foodhyd.2012.10.006>
- Zhang, L., Zhao, L., Bian, X., Guo, K., Zhou, L., & Wei, C. (2018). Characterization and comparative study of starches from seven purple sweet potatoes. *Food Hydrocolloids*, 80, 168–176. <https://doi.org/10.1016/j.foodhyd.2018.02.006>
- Zhao, X., Andersson, M., & Andersson, R. (2018). Resistant starch and other dietary fiber components in tubers from a high-amylose potato. *Food Chemistry*, 251, 58–63. <https://doi.org/10.1016/j.foodchem.2018.01.028>
- Zhu, F., & Liu, P. (2020). Starch gelatinization, retrogradation, and enzyme susceptibility of retrograded starch: Effect of amylopectin internal molecular structure. *Food Chemistry*, 316, Article 126036. <https://doi.org/10.1016/j.foodchem.2019.126036>
- Zou, T., Song, H., Chu, X., Tong, L., Liang, S., Gong, S., et al. (2019). Efficient induction of gynogenesis through unfertilized ovary culture with winter squash (*Cucurbita maxima* Duch.) and pumpkin (*Cucurbita moschata* Duch.). *Scientia Horticulturae*, 264, Article 109152. <https://doi.org/10.1016/j.scienta.2019.109152>